Draft version August 1, 2025
Typeset using LaTeX default style in AASTeX631

AGN Feedback Efficiency of NAL Quasars

Toru Misawa [1], Jane C. Charlton [2], and Michael Eracleous [2,3]

[1] Center for General Education, Shinshu University, 3-1-1 Asahi, Matsumoto, Nagano 390-8621, Japan
[2] Department of Astronomy and Astrophysics, Penn State University, 525 Davey Lab, 251 Pollock Road, University Park, PA 16802
[3] Institute for Gavitation and the Cosmos, Penn State University, University Park, PA 16802

ABSTRACT

We consider if outflowing winds that are detected via narrow absorption lines (NALs) with FWHM of < 500 km s^{-1} (i.e., NAL outflows) in quasar spectra contribute to feedback. As our sample, we choose 11 NAL systems in eight optically luminous quasars from the NAL survey of Misawa et al. (2007a), based on the following selection criteria: i) they exhibit "partial coverage" suggesting quasar origin (i.e., *intrinsic* NALs), ii) they have at least one low-ionization absorption line (C II and/or Si II), and iii) the Lyα absorption line is covered by available spectra. The results depend critically on this selection method, which has caveats and uncertainties associated with it, as we discuss in a dedicated section of the paper. Using the column density ratio of the excited and ground states of C II and Si II, we place upper limits on the electron density as $n_{\rm e} < 0.2$–18 cm^{-3} and lower limits on their radial distance from the flux source R as greater than several hundreds of kpc. We also calculate lower limits on the mass outflow rate and kinetic luminosity of $\log(\dot{M}/{\rm M}_\odot\ {\rm s}^{-1}) > 79$–$(3.1\times10^5)$ and $\log(\dot{E}_{\rm k}/{\rm erg\ s}^{-1}) > 42.9$–$49.8$, respectively. Taking the NAL selection and these results at face value, the inferred feedback efficiency can be comparable to or even larger than those of broad absorption line and other outflow classes, and large enough to generate significant AGN feedback. However, the question of the connection of quasar-driven outflows to NAL absorbers at large distances from the central engine remains open and should be addressed by future theoretical work.

Keywords: Quasar absorption line spectroscopy (1317) — Quasars(1319) — AGN host galaxies(2017)

1. INTRODUCTION

Outflowing winds from active galactic nuclei (AGN) deposit energy and momentum into the interstellar medium (ISM) and circum-galactic medium and regulate the star formation activity of their host galaxies. This could contribute significantly to the evolution of the host galaxies (i.e., AGN feedback; Silk & Rees 1998; Scannapieco & Oh 2004; Choi et al. 2018), if the total kinetic luminosity of the outflowing winds is larger than ∼0.5% (Hopkins & Elvis 2010) or ∼5% (Scannapieco & Oh 2004; Di Matteo et al. 2005) of the quasar's Eddington luminosity.

AGN outflowing winds are often found via broad absorption lines (BALs) with line widths of $\geq 2{,}000$ km s^{-1} in the spectra of about 15–40% of optically selected quasars (e.g., Weymann et al. 1991; Knigge et al. 2008; Dai et al. 2008; Gibson et al. 2009; Allen et al. 2011). Their ejection velocities from the quasars ($v_{\rm ej}$) range from several hundreds up to 30,000 km s^{-1} or more (Weymann et al. 1991; Rodríguez Hidalgo et al. 2020; Hamann et al. 2018).

Powerful outflows of several quasars with BALs (i.e., BAL quasars) have kinetic luminosities that satisfy the above feedback conditions (e.g., Arav et al. 2013; Borguet et al. 2013; Xu et al. 2019; Byun et al. 2022a; Choi et al. 2020; Walker et al. 2022). Significant feedback is especially likely for extremely high-velocity outflows (EHVOs) with outflow velocities of $\sim 0.1c$–$0.2c$ (e.g., Rodríguez Hidalgo et al. 2020; Vietri et al. 2022), similar to the Ultra Fast Outflows (UFOs) that are often detected via absorption lines in the X-ray spectra of AGNs (Tombesi et al. 2010; Gofford et al. 2013).

Corresponding author: Toru Misawa
misawatr@shinshu-u.ac.jp

In addition to BALs, narrow absorption lines (NALs) with line widths of $\leq$ 500 km s^{-1} and their intermediate subclass (mini-BALs) with line widths of 500 – 2000 km s^{-1} have been used to study AGN outflowing winds (Misawa et al. 2007a; Nestor et al. 2008; Hamann et al. 2011; Ganguly et al. 2013; Culliton et al. 2019; Dehghanian et al. 2024). A substantial fraction of NALs found in quasar spectra do not arise in gas that is physically related to the quasars themselves (*intervening* NALs, hereafter); they arise in cosmologically intervening absorbers such as foreground galaxies, the intergalactic medium, and Milky Way gas. But some fraction of NALs have been associated with quasar outflows (*intrinsic* NALs, hereafter) based partly on the following statistical arguments: 1) the detection rate of NALs varies depending on the physical properties of the background quasars (e.g., optical and radio luminosity, radio spectral index, and radio morphology; Richards et al. 1999; Richards 2001) and 2) a significant fraction of NALs remains after accounting for the contributions from cosmologically intervening absorbers and absorbers associated with quasar host galaxies or their cluster environment (Nestor et al. 2008; Wild et al. 2008). Additional arguments for such an association include time variability, partial coverage, or line-locking exhibited by *some* NALs (Hamann et al. 1997b; Lewis & Chelouche 2023). However, identifying specific intrinsic NALs is not straightforward because they do not display all the traits of other intrinsic absorption systems, such as BALs and mini-BALs, at the same time. Some NALs do vary (a fraction of $\sim$20–25%; e.g., Wise et al. 2004; Narayanan et al. 2004) and some display partial coverage (e.g., Misawa et al. 2007a). NALs that do display partial coverage do not do so in all the transitions from the same system. Therefore, the selection of samples of intrinsic NALs has some inherent ambiguity and any sample selected by these criteria may be contaminated by intervening NALs. (we return to these issues in §3 and discuss how they affect the work presented here). In view of the properties described just above, any NALs that may be intrinsic are unlikely to be associated with the same portions/regions of quasar outflows that produce BALs and mini-BALs (for example, Ganguly et al. 2001, associated the NAL gas with different layers of the outflow than the BAL gas; alternatively the NAL gas may be at a different distance from the central engine than the BAL gas). Moreover, the structure of NAL absorbers is likely to be different from the structure of BAL and mini-BAL absorbers; in fact NAL absorbers have been suggested to be filaments with an inner, low-ionization "core" surrounded by an outer, tenuous, higher-ionization layer (e.g., Culliton et al. 2019) in order to explain the detection of partial coverage in only some transitions from the same system.

There are two possible interpretations of the fraction of quasars hosting BALs, NALs, and mini-BALs. The first is an orientation scenario, in which BALs are observed if our line of sight (LoS) to the continuum source passes through the main, dense stream of the outflowing wind (e.g., Elvis 2000; Ganguly et al. 2001; Hamann et al. 2012). In this scenario, the difference in line width could depend the inclination angle of our LoS relative to the outflow direction or on the distance of the gas producing the different absorption lines from the continuum source. The latter possibility is bolstered by the association of blueshifted absorption lines with outflowing gas at a wide range of distances from the continuum source, from parsecs to hundreds of kilo-parsecs (e.g., de Kool et al. 2001; Chamberlain et al. 2015; Itoh et al. 2020). An alternative idea is the evolution scenario, in which BAL quasars are in an evolutionary stage (e.g., just after galaxy merging) in which they are obscured by dust (Farrah et al. 2007; Lípari & Terlevich 2006). This scenario is supported by the observation that the BAL quasar fraction, outflow velocity, and line width of absorption lines at $z_{\rm abs} \geq 6$ are a few times larger than those at lower redshift (Bischetti et al. 2022, 2023).

The physical parameters of outflowing winds have been studied through variability of the strengths and profiles of the absorption lines, since almost all BALs and mini-BALs vary over a few years in the quasar's rest frame (e.g., Gibson et al. 2008; Misawa et al. 2014; Capellupo et al. 2012). The probability of variation increases with the time interval between observations, approaching unity for intervals of a few years (Capellupo et al. 2013). When multiple BAL troughs are present, they often tend to vary in a coordinated fashion (e.g., Filiz Ak et al. 2013; Hemler et al. 2019). In extreme cases, BAL profiles appear or disappear (e.g., Filiz Ak et al. 2012; McGraw et al. 2017; Sameer et al. 2019). Possible origins of such variations include (a) motion of the absorbing gas parcels across our line of sight and (b) changes in the ionization state of the absorber (e.g., Hamann et al. 2008; Misawa et al. 2007b; Rogerson et al. 2016; Huang et al. 2019; Vietri et al. 2022).

In past studies, the mass flow rate ($\dot{M}$) and kinetic luminosity ($\dot{E}_{\rm k}$) of outflowing winds have been estimated as follows: 1) the electron number density ($n_{\rm e}$) is determined using measurements of troughs from excited states (e.g., Hamann et al. 2001; Borguet et al. 2012), or from the variability time scale of BALs and mini-BALs (e.g., Hamann et al. 1997c; Misawa et al. 2005), 2) the ionization parameter (U) and total Hydrogen column density ($N_{\rm H}$) are determined by comparing the observed column densities of various ions to simulated values using photoionization models (e.g., Xu et al. 2018; Miller et al. 2020; Walker et al. 2022), 3) the radial distance of the absorber from the center (R) is then

obtained from the values of n_e and U (e.g., Narayanan et al. 2004; Rogerson et al. 2016), and 4) the knowledge of R, N_H and the velocity of the outflow (v_{ej}) allows us to determine the mass flow rate ($\dot{M}$) and kinetic luminosity ($\dot{E}_k$) of a given outflow (see §3 and 4 for details).

While the feedback efficiency of BALs and mini-BALs have been studied in detail, those of NALs have hardly been examined because most NALs are so stable that we cannot extract information from time-variability analysis. However, NALs potentially have large values of $\dot{M}$ ($\propto v_{ej}$) and $\dot{E}_k$ ($\propto v_{ej}^3$) and could contribute significantly to AGN feedback since they appear to be more common (∼50%) and have larger outflow velocities (up to ∼0.2c) compared to BAL and mini-BALs (Misawa et al. 2007a).

In recent years, $\dot{M}$ and $\dot{E}_k$ of AGN outflows have been evaluated using absorption lines from ground states (i.e., resonance lines) and excited states of ions such as C II, Si II, O IV, and Ne V (e.g., Arav et al. 2018; Byun et al. 2022a, 2024). This method has two advantages over time-variability analysis: i) it requires only a single-epoch spectrum and ii) it can be applied to absorption lines that do not vary, such as NALs.

In this study, we investigate the feedback efficiency of quasars using intrinsic NAL absorbers, in contrast to past studies that focused on BALs and mini-BALs. We select intrinsic NAL candidates using their partial coverage signature, which is subject to caveats. We calculate the physical parameters using excited and ground state absorption lines instead of time-variability analysis. We describe the sample selection in §2 and discuss its caveats in §3, respectively. We present the analysis in §4 and our results and discussion in §5. Finally, §6 summarizes our work. Throughout the paper, we use a cosmology with H_0=69.6 km s^{-1} Mpc^{-1}, Ω_m=0.286, and Ω_Λ=0.714 (Bennett et al. 2014).

2. SAMPLE SELECTION

In this work we rely on partial coverage analysis to select quasars with intrinsic NALs. This selection method involves several caveats, which we discuss in §3 but it is the only method that can yield a sample of quasars with available high-resolution spectra suited for the analysis that we carry out here. Misawa et al. (2007a) identified 39 intrinsic NAL candidates based on partial coverage analysis of C IV, N V, and Si IV doublets in the spectra of 20 bright quasars at z_{em} = 2–4. Since the sample searched included 37 quasars, at least 50% of quasars host intrinsic NALs. The detection limits in rest-frame equivalent width were EW_{lim}(C IV) = 0.056 Å, EW_{lim}(N V) = 0.038 Å, and EW_{lim}(Si IV) = 0.054 Å.

The quasars were originally selected for a survey aimed at measuring the Deuterium-to-Hydrogen abundance ratio (D/H) in the Lyα forest (e.g., Burles & Tytler 1998a,b). Therefore, the target selection does not have a direct bias with respect to the properties of any intrinsic absorption-line systems, although there could be indirect bias since the sample contains only optically bright quasars. The observations were carried out with Keck/HIRES with a slit width of 1.″14 (i.e., FWHM ∼8 km s^{-1}). The spectra were extracted with the automated program, MAKEE, written by Tom Barlow.

We focus on 16 intrinsic NAL candidates of the 39 absorption systems that have at least one low-ionization absorption line from an ion with ionization potential between 13 and 24 eV (e.g., O I, Si II, Al II, and C II). We reject two systems with large column densities of $\log N_{HI} > 19$ since there are several observational indicators suggesting that some (sub-)DLAs[1], contain small-sized and high-density clouds within themselves: e.g., occurrence of time-variation (Hacker et al. 2013) and emergence of absorption lines from ions in excited states (e.g., Wolfe et al. 2003).

Of the remaining 14 systems, we choose 11 systems in 8 quasars as our sample because i) they have C II and/or Si II NALs which are necessary for the excited/resonance line analysis, and ii) the Lyα absorption line of the system is covered by past observations which is necessary for measuring total column densities of the outflowing winds.

We use the software package MINFIT (Churchill 1997; Churchill et al. 2003) to fit absorption lines with Voigt profiles using the absorption redshift (z_{abs}), column density ($\log N$ in cm^{-2}), Doppler parameter (b in km s^{-1}), and covering factor (C_f) as free parameters.

The covering factor, C_f, is the fraction of photons from the background flux source that pass through the foreground absorber along our line of sight; it is a measure of the dilution of the depths of absorption lines and needs to be included to get the correct column density. We evaluate C_f as

$$C_f = \frac{(1 - R_r)^2}{1 + R_b - 2R_r}, \quad (1)$$

[1] Damped Lyα systems

Table 1. Sample Quasars

(1) quasar	(2) $z_{\rm em}$	(3) $m_{\rm V}$[a] (mag)	(4) $m_{\rm R}$[a] (mag)	(5) $\mathcal{R}$[b]	(6) $L_{\rm bol}$[c] (erg s^{-1})	(7) $M_{\rm BH}$[d] ($M_\odot$)	(8) $L_{\rm Edd}$[e] (erg s^{-1})
Q0805+0441	2.88	18.16		3115	1.74×10^{47}	$1.94^{+0.25}_{-0.21}\times10^{9}$	$2.45^{+0.32}_{-0.27}\times10^{47}$
HS1103+6416	2.191	15.42		<0.62	1.18×10^{48}	$2.36^{+0.31}_{-0.26}\times10^{10}$	$2.97^{+0.39}_{-0.32}\times10^{48}$
Q1107+4847	3.000	16.60		<1.95	1.24×10^{48}	$3.30^{+0.38}_{-0.32}\times10^{9}$	$4.16^{+0.48}_{-0.41}\times10^{47}$
Q1330+0108	3.510		18.56	<16.2	3.93×10^{47}	$1.69^{+0.22}_{-0.18}\times10^{9}$	$2.13^{+0.27}_{-0.23}\times10^{47}$
Q1548+0917	2.749	18.00		<6.96	4.20×10^{47}	$5.96^{+0.80}_{-0.66}\times10^{9}$	$7.51^{+1.00}_{-0.84}\times10^{47}$
Q1554+3749	2.664	18.19		<21.9	3.26×10^{47}	$3.54^{+0.44}_{-0.37}\times10^{9}$	$4.46^{+0.55}_{-0.46}\times10^{47}$
HS1700+6416	2.722	16.12		<1.24	2.09×10^{48}	$2.59^{+0.34}_{-0.28}\times10^{10}$	$3.27^{+0.42}_{-0.35}\times10^{48}$
HS1946+7658	3.051	16.20		<1.35	2.87×10^{48}	$8.93^{+1.03}_{-0.88}\times10^{9}$	$1.12^{+0.13}_{-0.11}\times10^{48}$

[a] Observed V- or R-band magnitude from Misawa et al. (2007a).

[b] Radio loudness parameter $\mathcal{R} = f_\nu(5\ {\rm GHz})/f_\nu(4400\ {\rm Å})$ from Misawa et al. (2007a).

[c] Bolometric luminosity. See discussion in §2.

[d] Black hole mass. See discussion in §2.

[e] Eddington luminosity.

where $R_{\rm b}$ and $R_{\rm r}$ are the residual fluxes at the blue and red members of a doublet in the normalized spectrum (e.g., Wampler et al. 1995; Barlow & Sargent 1997; Hamann et al. 1997c). If $C_{\rm f} < 1$, the absorbers are likely arising in quasar outflowing winds (i.e., intrinsic absorbers) because cosmologically intervening absorbers like the CGM of foreground galaxies and the IGM have sizes much larger than the quasar continuum source. Based on the results of the covering factor analysis, Misawa et al. (2007a) separated all NALs into three classes: classes A and B were deemed to include reliable and possible intrinsic NALs and class C was taken to include intervening or unclassified NALs. The detailed classification criteria of each class are summarized in Misawa et al. (2007a).

The properties of the quasars in our sample are summarized in Table 1. Columns (1) and (2) are the quasar name and emission redshift ($z_{\rm em}$). Columns (3) and (4) give the V- and R-band magnitudes ($m_{\rm V}$ and $m_{\rm R}$, respectively). Columns (5)–(8) list the radio-loudness parameter ($\mathcal{R}$), the bolometric luminosity ($L_{\rm bol}$), the mass of the quasar's supermassive black hole ($M_{\rm BH}$), and the Eddington luminosity ($L_{\rm Edd}$). We calculate the bolometric luminosity by $L_{\rm bol} = 4.4\lambda L_\lambda(1450{\rm Å})$ (c.f., Richards et al. 2006). We use SDSS spectra to measure the monochromatic luminosity at 1450Å except for HS1946+7658, for which we use the spectrum of Hagen et al. (1992). All spectra are corrected for Galactic extinction (Schlafly & Finkbeiner 2011; Cardelli et al. 1989) before measuring the observed flux. We estimate the BH mass from the FWHM of the C IV emission line, the C IV emission line blueshift relative to the systemic redshift, and $\lambda L_\lambda(1350{\rm Å})$ using the empirical relation of Coatman et al. (2017).

Table 2 gives the parameters of intrinsic NALs: column (1) gives the quasar name, column (2) the absorption redshift ($z_{\rm abs}$), column (3) the neutral Hydrogen column density ($\log N_{\rm HI}$), columns (4)–(6) the ion of the targeted absorption line (C II or Si II), and the corresponding column densities in the ground and excited states ($\log N_{\rm l}$ and $\log N_{\rm u}$), columns (7) and (8) the derived limit on the electron density ($n_{\rm e}$) and radial distance from the center (R), and column (9), the reliability class of the intrinsic NAL.

3. CAVEATS ASSOCIATED WITH THE SAMPLE SELECTION

The conclusions of this work depend critically on whether the NALs that we have selected are indeed intrinsic. As we noted in §1, NALs do not show all the properties that signal the association of BALs and mini-BALs with an

Table 2. Properties of NAL Outflows

(1) quasar	(2) z_{abs}	(3) $\log N_{HI}$[a] (cm^{-2})	(4) ION[b]	(5) $\log N_l$[c] (cm^{-2})	(6) $\log N_u$[c] (cm^{-2})	(7) n_e[d] (cm^{-3})	(8) R[e] (kpc)	(9) class[f]
Q0805+0441	2.6517	15.11	C II	13.25	<12.90	<14.38	>108	A
HS1103+6416	1.8919	15.53	Si II	13.45	<11.78	<18.37	>248	B
Q1107+4847	2.7243	15.50	C II	12.70	<12.26	<11.09	>328	A
Q1330+0108	3.1148	14.99	C II	12.52	<12.07	<10.78	>187	A
Q1548+0917	2.6082	18.00	C II	13.47	<12.31	<1.79	>475	B
	2.6659	15.26	C II	13.11	<12.46	<6.30	>253	A
	2.6998	15.70	C II	12.67	<12.24	<11.41	>188	A
Q1554+3749	2.3777	15.63	C II	13.38	<12.33	<2.33	>367	A
HS1700+6416	2.4330	18.33	C II	12.88	<12.02	<3.90	>717	B
HS1946+7658	2.8928	17.11	C II	12.34	<11.71	<6.64	>644	A
	3.0497	17.37	C II	13.44	<11.35	<0.20	>3712	A

[a] Column density of neutral Hydrogen.

[b] Ion for which the column density, electron density, and absorber's radial distance are reported in columns (5) – (8).

[c] Column densities of the ion in column (4) in the ground and excited states.

[d] Electron density of the ion in column (4).

[e] Absorber's radial distance, corresponding to the ion listed in column (4).

[f] NAL classification made in Misawa et al. (2007a).

outflowing wind. Therefore, we highlight here the uncertainties associated with the partial coverage analysis method that is the basis of our selection.

1. It is possible that compact, dense clouds in a low-ionization state can exist in over-dense regions in DLA and sub-DLA systems. This possibility is suggested by (a) studies that find variable NALs at large blueshifts from the quasars toward which they are observed (see Hacker et al. 2013), (b) NALs from low-ionization, dense clouds that may show partial coverage in a handful of DLA or sub-DLA systems[2] (see Jones et al. 2010), and by a variety of models for the ISM of galaxies that predict compact, low-ionization clouds (e.g., Pfenniger & Combes 1994; Wolfe et al. 2003; Glover & Mac Low 2007; Fujita et al. 2009). Such clouds could have sizes of a few AU and exhibit partial coverage, although our targets that exhibit partial coverage in higher-ionized species (i.e., C IV and Si IV) are likely to have larger sizes.

2. Intrinsic NALs that are identified based on partial coverage ($C_f < 1$) do not show any other evidence connecting them to intrinsic absorbers (e.g., time-variability and broad line width) as seen in BALs and mini-BALs. Therefore, we cannot corroborate that they are intrinsic by an additional and separate test.

3. Intrinsic NALs have a black (i.e., fully absorbed) Lyα trough ($C_f = 1$) while BAL and mini-BAL systems show a non-black Lyα trough ($C_f < 1$). Moreover, in most cases only one component in the intrinsic NAL systems we have selected shows $C_f < 1$ while the other components are consistent with $C_f = 1$.

[2] These systems also suffer from unresolved saturation, but photoionization models identify them as extremely dense and cold absorbers corresponding to the molecular gas in the Milky Way.

To guard against the first caveat, we exclude DLA and sub-DLA systems from our sample even if they show partial coverage. The second and third caveats introduce uncertainty in our selection of intrinsic NALs since we have to rely only on the partial coverage signature from one transition. Nonetheless, we do not that, (a) photoionization models for intervening absorbers that can produce C IV and Si IV lines typically have kpc-scale sizes (e.g., Stern et al. 2016; Sameer et al. 2024), and (b) intrinsic absorbers may have a dense, compact core that can produce partial coverage in some transitions and a more extended halo that can produce full coverage in others (see Culliton et al. 2019).

4. ANALYSIS

We calculate the mass outflow rate ($\dot{M}$), kinetic luminosity ($\dot{E}_{\rm k}$), and eventually the feedback efficiency following the prescription of Borguet et al. (2012). First, we need to estimate the absorber's radial distance from the ionizing continuum source (R), total Hydrogen column density ($N_{\rm H}$), and ejection velocity ($v_{\rm ej}$). Of these parameters, only $v_{\rm ej}$ is measured directly from the observed spectra.

We estimate the absorber's distance R based on the definition of the ionization parameter[3]

$$U = \frac{Q({\rm H})}{4\pi R^2 n_{\rm H} c}, \tag{2}$$

where $Q(H)$ is the total number of Hydrogen ionizing photons emitted per unit time, $n_{\rm H}$ is the Hydrogen number density, and c is the speed of light. In order to evaluate accurately the ionization parameter, it is necessary to use photoionization models. However, the number of absorption lines detected in these NAL systems is limited to only three elements (i.e., H, C, and Si) and the covering factor of single lines (i.e., Lyα, C II, and Si II) cannot be evaluated in practice, which prevents us from constraining the photoionization models effectively. Therefore, we instead assume $\log U = -2.6$ because that is the ionization state where the average value of the column density ratio[4] of C II and C IV in our NAL systems, N(C II)/N(C IV) ~ 0.3, is approximately reproduced (Hamann 1997a)[5]. We convert the quasar bolometric luminosity $L_{\rm bol}$ to $Q(H)$ using a conventional quasar SED that is a segmented power law, $f_\nu \propto \nu^{-\alpha}$, where $\alpha = 0.4$, 1.6, and 0.9 at $\log \nu = 13.5$–15.5, 15.5–17.5, and 17.5–19.5 Hz, respectively Narayanan et al. (2004).

We also need to know the absorber's Hydrogen number density $n_{\rm H}$, which is related to the absorber's electron density $n_{\rm e}$ as $n_{\rm e} \sim 1.2 n_{\rm H}$ in highly ionized plasma (Osterbrock & Ferland 2006). While Narayanan et al. (2004) used the variability time scale as an upper limit on the recombination time to estimate the electron density, we use the column density ratio of excited and ground states of C II and Si II following previous works (e.g., Arav et al. 2013; Byun et al. 2022a) since i) we have spectra from only a single epoch, and ii) intrinsic NALs are rarely variable (Misawa et al. 2014).

We estimate the total Hydrogen column density (i.e., $N_{\rm H\,I} + N_{\rm H\,II}$) from the neutral Hydrogen column density ($N_{\rm H\,I}$) using a Cloudy photoionization model (version c17.02, Ferland et al. 2017) with an ionization parameter of $\log U = -2.6$ and the conventional quasar SED as introduced above.

We also use the Voigt profile fitting code MINFIT to measure column densities as well as Doppler b parameters of ground and excited states of C II and Si II. We assume full coverage (i.e., $C_{\rm f} = 1$) because we cannot evaluate $C_{\rm f}$ for single lines. If $C_{\rm f} < 1$, our estimate, which assumes $C_{\rm f}$=1, is a lower limit on the column density. However, the estimated electron density ratio $N_{\rm l}/N_{\rm u}$ and the corresponding electron density would be insensitive to $C_{\rm f}$ unless the lines are saturated, as demonstrated in Figure 1. If the absorption lines require multiple components to fit their profiles, we only consider the strongest components for calculating electron densities. Using the column density ratio of the strongest components, we place constraints on the electron density using

$$n_{\rm e} = n_{\rm cr} \left[\frac{N_{\rm l}}{N_{\rm u}} \left(\frac{g_{\rm u}}{g_{\rm l}} \right) e^{-\Delta E/kT} - 1 \right]^{-1}, \tag{3}$$

where $n_{\rm cr}$ is the critical density, $N_{\rm l}$ and $N_{\rm u}$ are the column densities of the ground and excited states, $g_{\rm l}$ and $g_{\rm u}$ are their statistical weights ($g_{\rm u}/g_{\rm l} = 2$ for the relevant energy levels of C II and Si II), ΔE is the energy difference between ground and excited states, k is the Boltzmann constant, and T is gas temperature.

[3] The ionization parameter is defined as $U \equiv n_\gamma / n_{\rm H}$, where n_γ is ionizing photon density.

[4] The column densities of C II and C IV are evaluated by fitting Voigt profiles to their absorption troughs. We evaluate a column density of C II using the same covering factor as C IV. We also assume C II and C IV absorbers have same ionization parameter in a single-phase, since their absorption profiles are very similar with negligible velocity offset from each other.

[5] We also perform photoionization models ourselves for an optically thin cloud with solar abundance assuming a conventional quasar SED (Narayanan et al. 2004) and confirm that the ionization condition of $\log U = -2.6$ well reproduces the column density ratio of N(C II)/N(C IV) ~ 0.3.

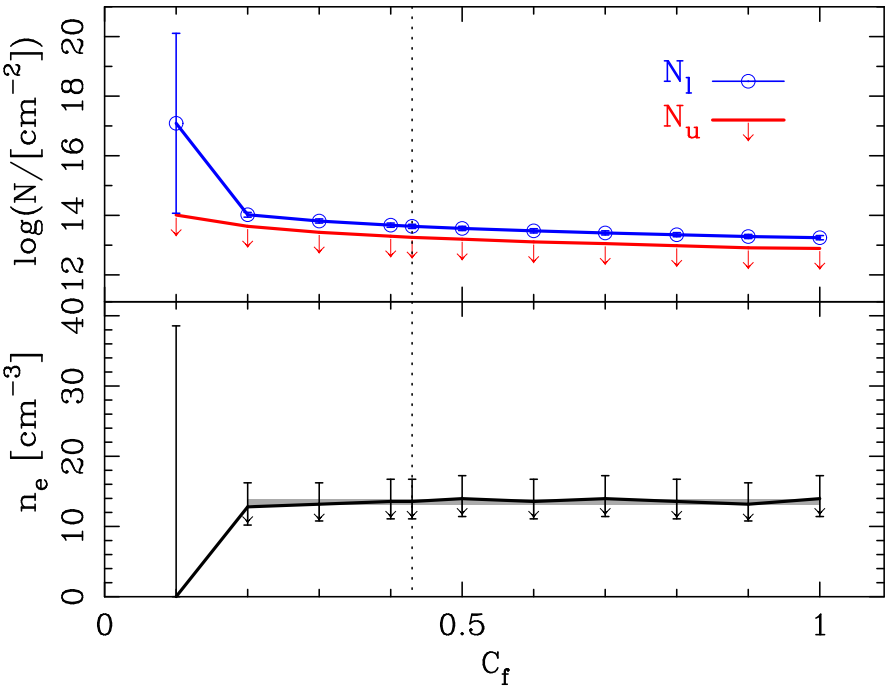

Figure 1. Estimated column densities of the ground and excited states ($N_{\rm l}$ and $N_{\rm u}$, respectively) of the C II line at $z_{\rm abs}$ = 2.6517 in the spectrum of Q0805+0441 (top panel) and their corresponding electron density (bottom panel) as an example demonstrating the lack of sensitivity of n_e to $C_{\rm f}$. The C IV line of the system has covering factor of $C_{\rm f} = 0.43$ (marked with a vertical dotted line), but the C II line could have different $C_{\rm f}$ value. Therefore, we estimate column densities of C II and C II* as a function of covering factor. We place only upper limits on N(C II*) and $n_{\rm e}$. For $C_{\rm f} \geq 0.2$, an upper limit of $n_{\rm e}$ is almost constant ($\leq 13.5 \pm 0.4$, considering only systematic errors) as shown with the shaded area on the bottom panel.

Since ΔE (1.26×10^{-14} erg and 5.69×10^{-14} erg for C II and Si II[6]) is much smaller than kT corresponding to the typical temperature of NAL systems (i.e., $T \sim 10^4$ K), the exponential part of equation (3) can be considered as ∼1. Using the critical densities of C II and Si II ($n_{\rm cr}$ ∼50 cm^{-3} and ∼1700 cm^{-3} for C II and Si II; Tayal 2008a,b), we can calculate the electron densities of the NAL systems.

We place only upper limits on the electron density, which we plot in Figure 2, since i) no lines in excited states (i.e., C II*1336, Si II*1265, Si II*1533) are detected while the corresponding lines in ground states are detected at a $\geq 3\sigma$ level (see Figure 3 as an example) and ii) the column densities of ground states are lower limits as described above. Similarly, we place lower limits on the NAL outflow radial distances using equation (3) of Narayanan et al. (2004) (see also our equation (2), above). If both C II and Si II lines are detected in a single NAL system, we prioritize the former because C II provides a stronger constraint. In addition to the low-ionization lines, we also evaluate line parameters of neutral Hydrogen (H I) using only the Lyα line[7].

The column densities of H I, C II, and Si II in ground and excited states (only upper limits at 1σ level), electron densities, and radial distances from the quasar continuum source of the 11 NAL absorbers are summarized in Table 2.

5. RESULTS & DISCUSSION

Using the parameters we evaluated in §2, we calculate the mass outflow rate and the kinetic luminosity following Borguet et al. (2012):

$$\dot{M} = 4\pi R f_{\rm c} \mu m_{\rm p} N_{\rm H} v_{\rm ej}, \tag{4}$$

$$\dot{E}_{\rm k} = \frac{1}{2}\dot{M} v_{\rm ej}^2 = 2\pi R f_{\rm c} \mu m_{\rm p} N_{\rm H} v_{\rm ej}^3, \tag{5}$$

[6] https://www.nist.gov/pml/atomic-spectra-database

[7] Although higher order Lyman series lines (e.g., Lyβ) are covered by some spectra of our sample quasars, their corresponding signal-to-noise ratio is very low.

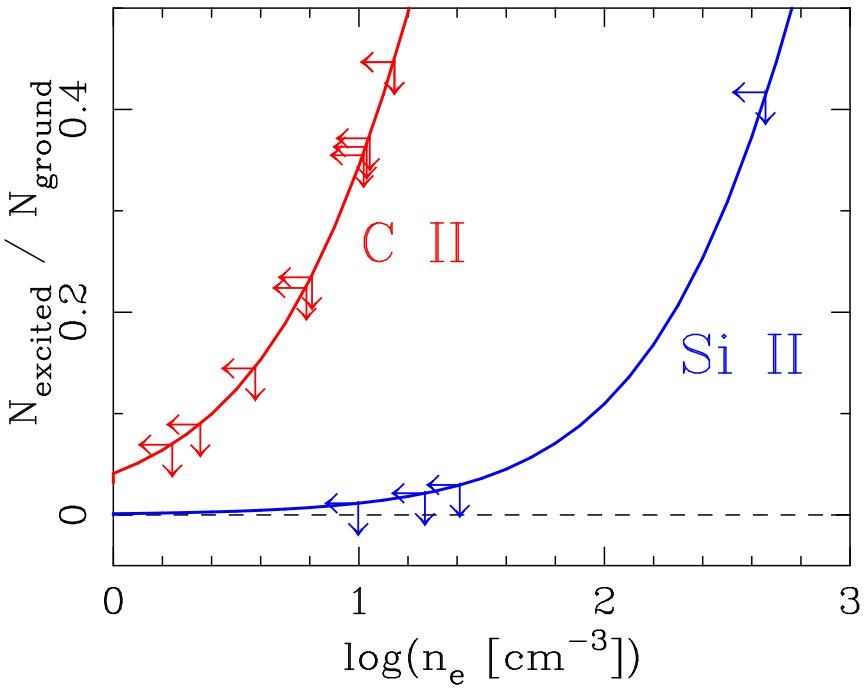

Figure 2. Column density ratios between excited and ground states of C II and Si II (red and blue curves) as a function of electron density, which is calculated with the CHIANTI 10.0 Database (Dere et al. 1997; Del Zanna et al. 2021) assuming a gas temperature of 10,000 K. Arrows denote upper limits on the column density ratio of C II* to C II and Si II* to Si II and the corresponding upper limits on electron density.

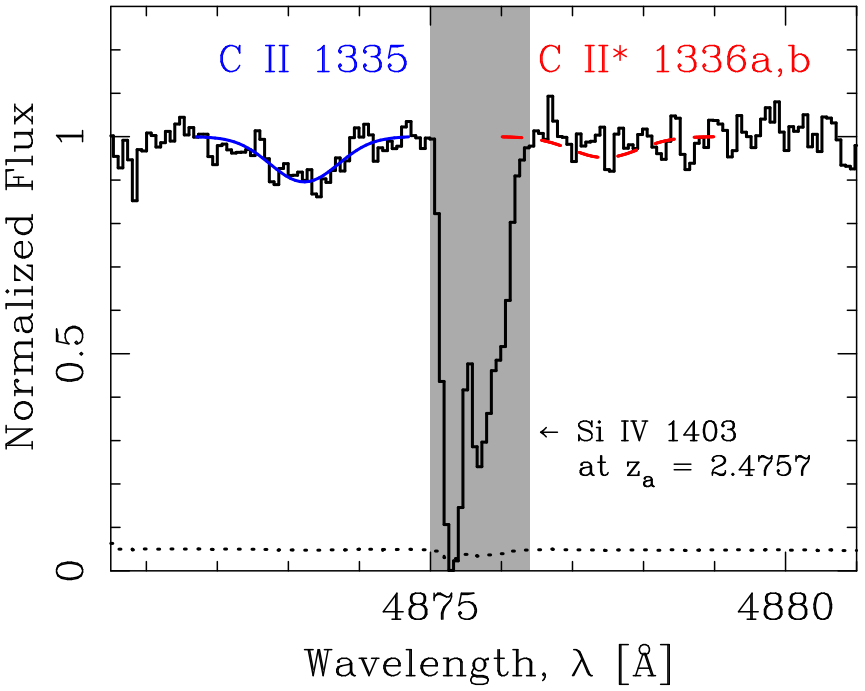

Figure 3. Normalized flux spectrum (solid histogram) and error spectrum (dotted histogram) around the absorption lines of C II 1335 and C II* 1336a,b at z_{abs} = 2.6517 in Q0805+0441. The former is detected at a 3σ level, while the latter is not detected. The blue solid curve is a fitted model to C II 1335. The red dashed curve is a 1-σ upper limit on C II* 1336a,b. The strong absorption profile in the gray shaded area is an unrelated Si IV 1403 line at z_{abs} = 2.4757.

Table 3. Feedback Efficiency of NAL outflows

(1) quasar	(2) $z_{\rm abs}$	(3) $\log N_{\rm H}{}^a$ ($\rm cm^{-2}$)	(4) $v_{\rm ej}$ ($\rm km\ s^{-1}$)	(5) $\dot{M}{}^b$ ($\rm M_\odot\ yr^{-1}$)	(6) $\dot{E}_{\rm k}{}^c$ ($\rm erg\ s^{-1}$)	(7) $\varepsilon_{\rm k}{}^d$
Q0805+0441	2.6517	17.75	18171	$>7.9\times10^{1}$	$>8.24\times10^{45}$	>0.043
HS1103+6416	1.8919	18.17	29437	$>7.8\times10^{2}$	$>2.12\times10^{47}$	>0.091
Q1107+4847	2.7243	18.14	21385	$>6.9\times10^{2}$	$>1.00\times10^{47}$	>0.047
Q1330+0108	3.1148	17.62	27433	$>1.5\times10^{2}$	$>3.65\times10^{46}$	>0.19
Q1548+0917	2.6082	20.33	11480	$>8.4\times10^{4}$	$>3.48\times10^{48}$	>7.8
	2.6659	17.90	6727	$>9.7\times10^{1}$	$>1.39\times10^{45}$	$>3.1\times10^{-3}$
	2.6998	18.34	3959	$>1.2\times10^{2}$	$>5.78\times10^{44}$	$>1.3\times10^{-3}$
Q1554+3749	2.3777	18.27	24356	$>1.2\times10^{3}$	$>2.23\times10^{47}$	>0.34
HS1700+6416	2.4330	20.40	24195	$>3.1\times10^{5}$	$>5.78\times10^{49}$	>22
HS1946+7658	2.8928	19.80	11942	$>3.5\times10^{4}$	$>1.57\times10^{48}$	>0.34
	3.0497	20.01	98	$>2.7\times10^{3}$	$>8.10\times10^{42}$	$>1.8\times10^{-6}$

[a] Total Hydrogen column density including both neutral and ionized Hydrogen.

[b] Mass outflow rate.

[c] Kinetic luminosity.

[d] Feedback efficiency, defined as the ratio of the NAL kinetic luminosity of the outflow to the Eddington luminosity of the quasar, $\dot{E}_{\rm k}/L_{\rm Edd}$. The values in this column assume the absorber distances in Table 2.

where $f_{\rm c}$ is the global covering fraction of the NAL outflow, μ (= 1.4) is the mean molecular weight, and $m_{\rm p}$ is the proton mass. We use $f_{\rm c} = 0.5$ since intrinsic NALs are identified at least 50% of optically luminous quasars (Misawa et al. 2007a). Since $f_{\rm c}$ was estimated based only on partial coverage analysis, we caution that it is uncertain. The kinetic luminosity and feedback efficiency estimated below are proportional to $f_{\rm c}$, therefore they would carry the same fractional uncertainty as $f_{\rm c}$. By substituting parameters in Table 2 into equations (4) and (5), we evaluate $\dot{M}$ and $\dot{E}_{\rm k}$ and summarize the results in Table 3.

The AGN feedback efficiency $\varepsilon_{\rm k}$ is computed as

$$\varepsilon_{\rm k} = \frac{\dot{E}_{\rm k}}{L_{\rm Edd}} = \frac{\dot{E}_{\rm k}}{4\pi G M_{\rm BH} m_{\rm p} c/\sigma_{\rm T}}, \tag{6}$$

where $L_{\rm Edd}$ is the Eddington luminosity, G is the gravitational constant, $M_{\rm BH}$ is the mass of the SMBH, and $\sigma_{\rm T}$ is the Thomson cross section. The feedback efficiencies of the 11 NAL systems in the eight quasars of this study are summarized in Table 3 and plotted in Figure 4.

We emphasize that the mass outflow rate, $\dot{M}$, the kinetic luminosity, $\dot{E}_{\rm k}$, and the AGN feedback efficiency, $\varepsilon_{\rm k}$, reported above are lower limits for the following reasons: i) equations (4) and (5) provide lower limits on $\dot{M}$ and $\dot{E}_{\rm k}$ if outflows are instantaneous (not continuous) with volume filling factors of $f_{\rm V} < 1$ (see §5 of Borguet et al. 2012) and ii) the radial distances of the absorbers, R, listed in Table 2 are lower limits since we obtain only upper limits on the electron density $n_{\rm e}$ without detecting any C II and Si II lines in excited states.

Eight of the 11 NAL systems have lower limits of the feedback efficiency that are large enough to cause significant AGN feedback (i.e., $\varepsilon_{\rm k} > 0.005$). Among them, the systems at $z_{\rm abs} = 2.6082$ in Q1548+0917 and at $z_{\rm abs} = 2.4330$ in HS1700+6416 have extremely large feedback efficiencies greater than 7, which is due to their relatively large Hydrogen column densities (i.e., $\log N_{\rm H} > 20.3$). In contrast, those at $z_{\rm abs} = 2.6659$ and 2.6998 in Q1548+0917 and at $z_{\rm abs} =$

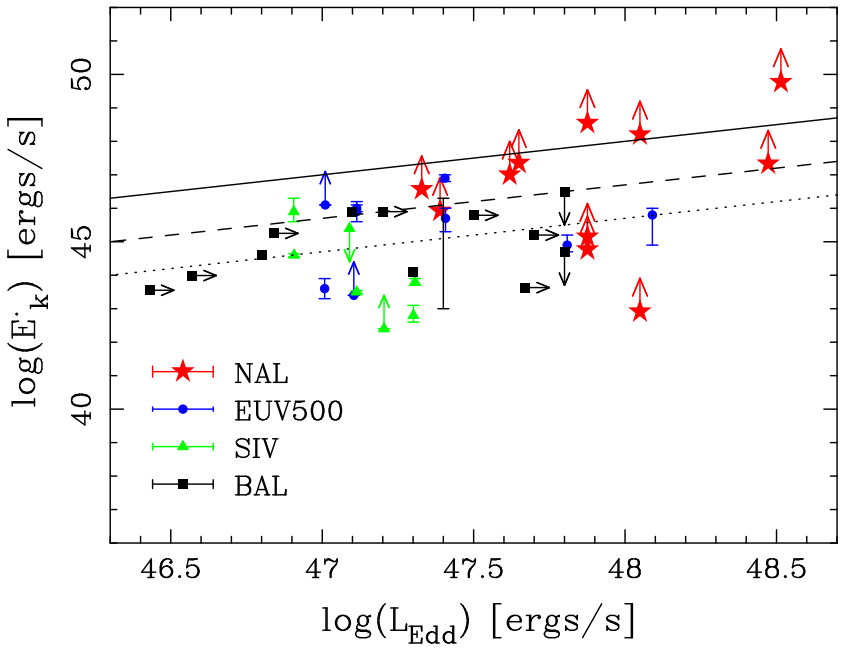

Figure 4. Kinetic luminosity ($\dot{E}_{\rm k}$) as a function of the Eddington luminosity ($L_{\rm Edd}$) for the 11 NAL systems of this study (red), along with nine EUV500 (blue) and seven S IV (green) systems from Miller et al. (2020). Filled black squares denote BALs from the literature (Fiore et al. 2017; Capellupo et al. 2014; Leighly et al. 2018; Xu et al. 2020; Miller et al. 2020; Vietri et al. 2022). Upper limits (rather than lower limits) on $\dot{E}_{\rm k}$ are given for some S IV and BAL systems since they exhibit time variation. Thick, dashed, and dotted black lines are relations between $\dot{E}_{\rm k}$ and $L_{\rm Edd}$ for a feedback efficiency of 1, 0.05, and 0.005, respectively.

3.0497 in HS1946+7658 have relatively small feedback efficiencies. The lower limits on $\varepsilon_{\rm k}$ of these systems are smaller than 0.005, which is mainly a result of their small ejection velocities (i.e., $v_{\rm ej} < 7{,}000$ km s^{-1}).

We also compare our result to past studies whose targets are i) BALs (Fiore et al. 2017; Capellupo et al. 2014; Leighly et al. 2018; Xu et al. 2020; Miller et al. 2020; Vietri et al. 2022), ii) highly-ionized S IV outflows whose ionization potential (IP) is 47.3 eV (Miller et al. 2020), and very high-ionized outflows hosting ions with IP of more than 100 eV (e.g., Ne VIII, Na IX, and Mg X) whose rest-frame absorption wavelengths are in the extreme-UV region between 500 and 1050 Å (EUV500; Miller et al. 2020). As shown in Figure 4, NAL outflows have an exceptionally large efficiency compared to the other outflow classes.

Before closing the discussion, we would like to emphasize that, the radial distances of NAL outflows we derived in §2 (from about 100 kpc and up to 4 Mpc) are much larger than the typical distances of BAL and mini-BAL outflows. The distances of BAL and mini-BAL outflows have been estimated based on i) time-variability analysis, ii) photoionization modeling, and iii) excited/resonance line analysis similar to that employed in this study, and are found to range from (sub-)parsec (Capellupo et al. 2014; Leighly et al. 2018; Xu et al. 2020) to tens of kilo-parsec (Hamann et al. 2001; Byun et al. 2022a,b; Walker et al. 2022). In contrast, since NALs are generally not observed to vary (Misawa et al. 2014) the radial distances of NAL outflows have been constrained using only the last two of the above methods. Thus, NAL outflows in nearby Seyfert galaxies are found to be located at distances of several to to $\sim$ 10 kpc from the central engine (e.g., Dunn et al. 2010; Borguet et al. 2012). Estimates of distances of NAL outflows in high-z quasars vary significantly. For example, photoionization modeling has suggested a wide range of distances from pc to several kpc for NAL absorbers (even in the same quasar; Wu et al. 2010) while methods similar to those used here have suggested distances greater than $\sim$ 100 kpc (Itoh et al. 2020). Our results here imply even larger radial distances of that absorbing gas (i.e., several hundreds of kpc), which place the NAL outflows away from the immediate vicinity of the quasar central engine and in the outskirts of the host galaxy or in the CGM (cf. Faucher-Giguère et al. 2012; Itoh et al. 2020). The small filaments that produce the NALs may result from the interaction of a quasar-launched blast wave with dense gas in the host galaxy, as suggested by Faucher-Giguère et al. (2012). These large distances raise the question of the connection between fast, outflowing absorbers to the quasar central engine. Future work should

examine whether the NAL outflowing winds indeed have traveled such a long distance from the quasar's innermost regions to the scale of CGM and IGM, if NALs originate in compact parcels of gas expelled from the quasar host galaxies by quasar-driven outflows, and if other NALs "without" low-ionized species have a different origin (i.e., a different radial distance from the flux source).

6. SUMMARY AND CONCLUSIONS

In this study, we investigate the physical conditions of NAL outflows to test whether they contribute to AGN feedback. We carefully choose 11 NAL systems in eight quasars from Misawa et al. (2007a), and search for excited lines of C II and Si II ions to place constraints on their electron densities and radial distances from the continuum source. Although no lines from excited states are detected, we place lower limits on the mass outflow rates, kinetic luminosities, and feedback efficiencies of NAL outflows for the first time. Our main results are as follows:

- We study 11 NAL systems that were identified as intrinsic based on partial coverage analysis. We reiterate here that the selection method has caveats and uncertainties associated with it, which we discuss in §3. We also note that because the properties of intrinsic NALs are different from those of BALs and mini-BALs, the corresponding absorbers are probably associated with a different part or phase of the quasar outflow.

- The outflows traced by intrinsic NALs have large mass ejection rates, kinetic luminosities, and feedback efficiencies, namely $\log(\dot{M}/\mathrm{M}_\odot\ \mathrm{yr}^{-1}) > 79$–$3.1\times10^5$, $\log(\dot{E}_\mathrm{k}/\mathrm{erg\ s}^{-1}) > 42.9$–$49.8$, and $\varepsilon_\mathrm{k} \gtrsim 0$–$22$.

- Eight of the 11 cases studied here have feedback efficiencies greater than 0.5% (Hopkins & Elvis 2010), implying that they contribute significantly to AGN feedback.

- The feedback efficiency of some NAL outflows is larger than those of other outflow classes including BALs, high-ionized S IV, and very high-ionized EUV500 outflows. Such high efficiencies suggest that the outflows traced by NALs could deliver significant feedback from the quasar to the host galaxy.

- The radial distances of NAL outflows are estimated to be very large (i.e., hundreds of kilo-parsecs), which is larger than the typical distance of BAL outflows of 1 pc – 10 kpc. This result raises the question of what is the connection of the outflows traced by NALs to the quasar central engine. Do intrinsic NALs trace the portion of the outflow that has already left the quasar host galaxy? The connection has to be understood before we can fully evaluate how the NAL gas fits into the bigger picture of quasar-driven outflows.

- Taking these results at face value, we conclude that we need to take NAL outflows into account for estimating AGN feedback efficiency. However, additional work is needed to confirm the connection of NALs with partial coverage to quasar-driven outflows and to corroborate the results presented here.

For further investigation, we should obtain UV spectra of our sample quasars to detect a number of metal absorption lines (both from the ground states and excited states) in NAL systems, and place more stringent constraints on their electron densities and radial distances.

Our sample consists of only luminous quasars with bolometric luminosity of $\log(L_\mathrm{bol}/\mathrm{erg\ s}^{-1}) > 47.2$, which could bias the results in two ways: i) luminous quasars have larger outflow velocity, mass outflow rate, kinetic luminosity, and feedback efficiency (Ganguly & Brotherton 2008; Fiore et al. 2017; Bruni et al. 2019), and ii) luminous quasars over-ionize the CGM and the IGM around them both in the line-of-sight (Bajtlik et al. 1988; Scott et al. 2000) and transverse (Prochaska et al. 2013; Jalan et al. 2019; Misawa et al. 2022) directions. By observing a number of fainter quasars to increase the sample size, we will be able to study quasar feedback more generally. Moreover, we will increase the chances of detecting C II and Si II NALs in their excited states, which will help us get a more detailed understanding of the feedback efficiency of NAL outflows.

We would like to thank the anonymous referee for comments that helped us improve the paper. We also would like to thank Christopher Churchill for providing us with the MINFIT software packages. This work was supported by JSPS KAKENHI Grant Number 25K01038.

The data presented herein were obtained at the W. M. Keck Observatory, which is operated as a scientific partnership among the California Institute of Technology, the University of California and the National Aeronautics and Space Administration. The Observatory was made possible by the generous financial support of the W. M. Keck Foundation. The authors wish to recognize and acknowledge the very significant cultural role and reverence that the summit of MaunaKea has always had within the indigenous Hawaiian community. We are most fortunate to have the opportunity to conduct observations from this mountain. This work was supported by JSPS KAKENHI Grant Number 21H01126.

Funding for the Sloan Digital Sky Survey IV has been provided by the Alfred P. Sloan Foundation, the U.S. Department of Energy Office of Science, and the Participating Institutions. SDSS-IV acknowledges support and resources from the Center for High Performance Computing at the University of Utah. The SDSS website is www.sdss.org.

SDSS-IV is managed by the Astrophysical Research Consortium for the Participating Institutions of the SDSS Collaboration including the Brazilian Participation Group, the Carnegie Institution for Science, Carnegie Mellon University, Center for Astrophysics — Harvard & Smithsonian, the Chilean Participation Group, the French Participation Group, Instituto de Astrofísica de Canarias, The Johns Hopkins University, Kavli Institute for the Physics and Mathematics of the Universe (IPMU) / University of Tokyo, the Korean Participation Group, Lawrence Berkeley National Laboratory, Leibniz Institut für Astrophysik Potsdam (AIP), Max-Planck-Institut für Astronomie (MPIA Heidelberg), Max-Planck-Institut für Astrophysik (MPA Garching), Max-Planck-Institut für Extraterrestrische Physik (MPE), National Astronomical Observatories of China, New Mexico State University, New York University, University of Notre Dame, Observatário Nacional / MCTI, The Ohio State University, Pennsylvania State University, Shanghai Astronomical Observatory, United Kingdom Participation Group, Universidad Nacional Autónoma de México, University of Arizona, University of Colorado Boulder, University of Oxford, University of Portsmouth, University of Utah, University of Virginia, University of Washington, University of Wisconsin, Vanderbilt University, and Yale University.

REFERENCES

Allen, J. T., Hewett, P. C., Maddox, N., et al. 2011, MNRAS, 410, 860. doi:10.1111/j.1365-2966.2010.17489.x

Arav, N., Borguet, B., Chamberlain, C., et al. 2013, MNRAS, 436, 3286. doi:10.1093/mnras/stt1812

Arav, N., Liu, G., Xu, X., et al. 2018, ApJ, 857, 60. doi:10.3847/1538-4357/aab494

Bajtlik, S., Duncan, R. C., & Ostriker, J. P. 1988, ApJ, 327, 570. doi:10.1086/166217

Barlow, T. A. & Sargent, W. L. W. 1997, AJ, 113, 136. doi:10.1086/118239

Bennett, C. L., Larson, D., Weiland, J. L., et al. 2014, ApJ, 794, 135. doi:10.1088/0004-637X/794/2/135

Bischetti, M., Fiore, F., Feruglio, C., et al. 2023, ApJ, 952, 44. doi:10.3847/1538-4357/accea4

Bischetti, M., Feruglio, C., D'Odorico, V., et al. 2022, Nature, 605, 244. doi:10.1038/s41586-022-04608-1

Borguet, B. C. J., Edmonds, D., Arav, N., et al. 2012, ApJ, 751, 107. doi:10.1088/0004-637X/751/2/107

Borguet, B. C. J., Arav, N., Edmonds, D., et al. 2013, ApJ, 762, 49. doi:10.1088/0004-637X/762/1/49

Bruni, G., Piconcelli, E., Misawa, T., et al. 2019, A&A, 630, A111. doi:10.1051/0004-6361/201834940

Burles, S. & Tytler, D. 1998a, ApJ, 499, 699. doi:10.1086/305667

Burles, S. & Tytler, D. 1998b, ApJ, 507, 732. doi:10.1086/306341

Byun, D., Arav, N., Sharma, M., et al. 2024, A&A, 684, A158. doi:10.1051/0004-6361/202348215

Byun, D., Arav, N., & Hall, P. B. 2022a, ApJ, 927, 176. doi:10.3847/1538-4357/ac503d

Byun, D., Arav, N., & Hall, P. B. 2022b, MNRAS, 517, 1048. doi:10.1093/mnras/stac2638

Capellupo, D. M., Hamann, F., & Barlow, T. A. 2014, MNRAS, 444, 1893. doi:10.1093/mnras/stu1502

Capellupo, D. M., Hamann, F., Shields, J. C., et al. 2013, MNRAS, 429, 1872. doi:10.1093/mnras/sts427

Capellupo, D. M., Hamann, F., Shields, J. C., et al. 2012, MNRAS, 422, 3249. doi:10.1111/j.1365-2966.2012.20846.x

Cardelli, J. A., Clayton, G. C., & Mathis, J. S. 1989, ApJ, 345, 245. doi:10.1086/167900

Chamberlain, C., Arav, N., & Benn, C. 2015, MNRAS, 450, 1085. doi:10.1093/mnras/stv572

Choi, H., Leighly, K. M., Terndrup, D. M., et al. 2020, ApJ, 891, 53. doi:10.3847/1538-4357/ab6f72

Choi, E., Somerville, R. S., Ostriker, J. P., et al. 2018, ApJ, 866, 91. doi:10.3847/1538-4357/aae076

Churchill, C. W. 1997, Ph.D. Thesis

Churchill, C. W., Vogt, S. S., & Charlton, J. C. 2003, AJ, 125, 98. doi:10.1086/345513

Coatman, L., Hewett, P. C., Banerji, M., et al. 2017, MNRAS, 465, 2120. doi:10.1093/mnras/stw2797

Culliton, C., Charlton, J., Eracleous, M., et al. 2019, MNRAS, 488, 4690. doi:10.1093/mnras/stz1642

Dai, X., Shankar, F., & Sivakoff, G. R. 2008, ApJ, 672, 108. doi:10.1086/523688

Dehghanian, M., Arav, N., Byun, D., et al. 2024, MNRAS, 527, 7825. doi:10.1093/mnras/stad3695

de Kool, M., Arav, N., Becker, R. H., et al. 2001, ApJ, 548, 609. doi:10.1086/318996

Del Zanna, G., Dere, K. P., Young, P. R., et al. 2021, ApJ, 909, 38. doi:10.3847/1538-4357/abd8ce

Dere, K. P., Landi, E., Mason, H. E., et al. 1997, A&AS, 125, 149. doi:10.1051/aas:1997368

Di Matteo, T., Springel, V., & Hernquist, L. 2005, Nature, 433, 604. doi:10.1038/nature03335

Dunn, J. P., Crenshaw, D. M., Kraemer, S. B., et al. 2010, ApJ, 713, 900. doi:10.1088/0004-637X/713/2/900

Elvis, M. 2000, ApJ, 545, 63. doi:10.1086/317778

Farrah, D., Lacy, M., Priddey, R., et al. 2007, ApJL, 662, L59. doi:10.1086/519492

Faucher-Giguère, C.-A., Quataert, E., & Murray, N. 2012, MNRAS, 420, 1347. doi:10.1111/j.1365-2966.2011.20120.x

Ferland, G. J., Chatzikos, M., Guzmán, F., et al. 2017, RMxAA, 53, 385. doi:10.48550/arXiv.1705.10877

Filiz Ak, N., Brandt, W. N., Hall, P. B., et al. 2013, ApJ, 777, 168. doi:10.1088/0004-637X/777/2/168

Filiz Ak, N., Brandt, W. N., Hall, P. B., et al. 2012, ApJ, 757, 114. doi:10.1088/0004-637X/757/2/114

Fiore, F., Feruglio, C., Shankar, F., et al. 2017, A&A, 601, A143. doi:10.1051/0004-6361/201629478

Fujita A., Martin C. L., Mac Low M.-M., New K. C. B., Weaver R., 2009, ApJ, 698, 693. doi:10.1088/0004-637X/698/1/693

Ganguly, R., Lynch, R. S., Charlton, J. C., et al. 2013, MNRAS, 435, 1233. doi:10.1093/mnras/stt1366

Ganguly, R. & Brotherton, M. S. 2008, ApJ, 672, 102. doi:10.1086/524106

Ganguly, R., Bond, N. A., Charlton, J. C., et al. 2001, ApJ, 549, 133. doi:10.1086/319082

Gibson, R. R., Jiang, L., Brandt, W. N., et al. 2009, ApJ, 692, 758. doi:10.1088/0004-637X/692/1/758

Gibson, R. R., Brandt, W. N., Schneider, D. P., et al. 2008, ApJ, 675, 985. doi:10.1086/527462

Glover S. C. O., Mac Low M.-M., 2007, ApJ, 659, 1317. doi:10.1086/512227

Gofford, J., Reeves, J. N., Tombesi, F., et al. 2013, MNRAS, 430, 60. doi:10.1093/mnras/sts481

Hacker, T. L., Brunner, R. J., Lundgren, B. F., et al. 2013, MNRAS, 434, 163. doi:10.1093/mnras/stt1022

Hagen, H.-J., Cordis, L., Engels, D., et al. 1992, A&A, 253, L5

Hamann, F., Chartas, G., Reeves, J., et al. 2018, MNRAS, 476, 943. doi:10.1093/mnras/sty043

Hamann, F., Simon, L., Rodriguez Hidalgo, P., et al. 2012, AGN Winds in Charleston, 460, 47. doi:10.48550/arXiv.1204.3791

Hamann, F., Kanekar, N., Prochaska, J. X., et al. 2011, MNRAS, 410, 1957. doi:10.1111/j.1365-2966.2010.17575.x

Hamann, F., Kaplan, K. F., Rodríguez Hidalgo, P., et al. 2008, MNRAS, 391, L39. doi:10.1111/j.1745-3933.2008.00554.x

Hamann, F. W., Barlow, T. A., Chaffee, F. C., et al. 2001, ApJ, 550, 142. doi:10.1086/319733

Hamann, F. 1997a, ApJS, 109, 279. doi:10.1086/312980

Hamann, F., Barlow, T. A., Junkkarinen, V., et al. 1997b, ApJ, 478, 80. doi:10.1086/303781

Hamann, F., Barlow, T. A., & Junkkarinen, V. 1997c, ApJ, 478, 87. doi:10.1086/303782

Hemler, Z. S., Grier, C. J., Brandt, W. N., et al. 2019, ApJ, 872, 21. doi:10.3847/1538-4357/aaf1bf

Hopkins, P. F. & Elvis, M. 2010, MNRAS, 401, 7. doi:10.1111/j.1365-2966.2009.15643.x

Huang, H.-Y., Pan, C.-J., Lu, W.-J., et al. 2019, MNRAS, 487, 2818. doi:10.1093/mnras/stz1454

Itoh, D., Misawa, T., Horiuchi, T., et al. 2020, MNRAS, 499, 3094. doi:10.1093/mnras/staa2793

Jalan, P., Chand, H., & Srianand, R. 2019, ApJ, 884, 151. doi:10.3847/1538-4357/ab4191

Jones T. M., Misawa T., Charlton J. C., Mshar A. C., Ferland G. J., 2010, ApJ, 715, 1497. doi:10.1088/0004-637X/715/2/1497

Knigge, C., Scaringi, S., Goad, M. R., et al. 2008, MNRAS, 386, 1426. doi:10.1111/j.1365-2966.2008.13081.x

Leighly, K. M., Terndrup, D. M., Gallagher, S. C., et al. 2018, ApJ, 866, 7. doi:10.3847/1538-4357/aadee6

Lewis, T. R. & Chelouche, D. 2023, ApJ, 945, 110. doi:10.3847/1538-4357/acb541

Lípari, S. L. & Terlevich, R. J. 2006, MNRAS, 368, 1001. doi:10.1111/j.1365-2966.2006.10215.x

McGraw, S. M., Brandt, W. N., Grier, C. J., et al. 2017, MNRAS, 469, 3163. doi:10.1093/mnras/stx1063

Miller, T. R., Arav, N., Xu, X., et al. 2020, ApJS, 247, 39. doi:10.3847/1538-4365/ab5967

Misawa, T., Ishimoto, R., Kobu, S., et al. 2022, ApJ, 933, 239. doi:10.3847/1538-4357/ac7715

Misawa, T., Charlton, J. C., & Eracleous, M. 2014, ApJ, 792, 77. doi:10.1088/0004-637X/792/1/77

Misawa, T., Charlton, J. C., Eracleous, M., et al. 2007a, ApJS, 171, 1. doi:10.1086/513713

Misawa, T., Eracleous, M., Charlton, J. C., et al. 2007b, ApJ, 660, 152. doi:10.1086/513097

Misawa, T., Eracleous, M., Charlton, J. C., et al. 2005, ApJ, 629, 115. doi:10.1086/431342

Moravec, E. A., Hamann, F., Capellupo, D. M., et al. 2017, MNRAS, 468, 4539. doi:10.1093/mnras/stx775

Narayanan, D., Hamann, F., Barlow, T., et al. 2004, ApJ, 601, 715. doi:10.1086/380781

Nestor, D., Hamann, F., & Rodriguez Hidalgo, P. 2008, MNRAS, 386, 2055. doi:10.1111/j.1365-2966.2008.13156.x

Osterbrock, D. E. & Ferland, G. J. 2006, Astrophysics of gaseous nebulae and active galactic nuclei, 2nd. ed. by D.E. Osterbrock and G.J. Ferland. Sausalito, CA: University Science Books, 2006

Pfenniger D., Combes F., 1994, A&A, 285, 94. doi:10.48550/arXiv.astro-ph/9311044

Prochaska, J. X., Hennawi, J. F., Lee, K.-G., et al. 2013, ApJ, 776, 136. doi:10.1088/0004-637X/776/2/136

Richards, G. T., Lacy, M., Storrie-Lombardi, L. J., et al. 2006, ApJS, 166, 470. doi:10.1086/506525

Richards, G. T. 2001, ApJS, 133, 53. doi:10.1086/319183

Richards, G. T., York, D. G., Yanny, B., et al. 1999, ApJ, 513, 576. doi:10.1086/306894

Rodríguez Hidalgo, P., Khatri, A. M., Hall, P. B., et al. 2020, ApJ, 896, 151. doi:10.3847/1538-4357/ab9198

Rogerson, J. A., Hall, P. B., Rodríguez Hidalgo, P., et al. 2016, MNRAS, 457, 405. doi:10.1093/mnras/stv3010

Sameer, Charlton, J. C., Wakker, B. P., et al. 2024, MNRAS, 530, 4, 3827. doi:10.1093/mnras/stae962

Sameer, Brandt, W. N., Anderson, S., et al. 2019, MNRAS, 482, 1121. doi:10.1093/mnras/sty2718

Scannapieco, E. & Oh, S. P. 2004, ApJ, 608, 62. doi:10.1086/386542

Schlafly, E. F. & Finkbeiner, D. P. 2011, ApJ, 737, 103. doi:10.1088/0004-637X/737/2/103

Scott, J., Bechtold, J., Dobrzycki, A., et al. 2000, ApJS, 130, 67. doi:10.1086/317340

Silk, J. & Rees, M. J. 1998, A&A, 331, L1. doi:10.48550/arXiv.astro-ph/9801013

Stern, J., Hennawi, J. F., Prochaska, J. X., et al. 2016, ApJ, 830, 87. doi:10.3847/0004-637X/830/2/87

Tayal, S. S. 2008a, A&A, 486, 629. doi:10.1051/0004-6361:200810055

Tayal, S. S. 2008b, ApJS, 179, 534. doi:10.1086/591849

Tombesi, F., Cappi, M., Reeves, J. N., et al. 2010, A&A, 521, A57. doi:10.1051/0004-6361/200913440

Vestergaard, M. & Peterson, B. M. 2006, ApJ, 641, 689. doi:10.1086/500572

Vietri, G., Misawa, T., Piconcelli, E., et al. 2022, A&A, 668, A87. doi:10.1051/0004-6361/202243285

Walker, A., Arav, N., & Byun, D. 2022, MNRAS, 516, 3778. doi:10.1093/mnras/stac2349

Wampler, E. J., Chugai, N. N., & Petitjean, P. 1995, ApJ, 443, 586. doi:10.1086/175551

Wild, V., Kauffmann, G., White, S., et al. 2008, MNRAS, Narrow associated quasi-stellar object absorbers: clustering, outflows and the line-of-sight proximity effect, 388, 1, 227. doi:10.1111/j.1365-2966.2008.13375.x

Weymann, R. J., Morris, S. L., Foltz, C. B., et al. 1991, ApJ, 373, 23. doi:10.1086/170020

Wise, J. H., Eracleous, M., Charlton, J. C., et al. 2004, ApJ, Variability of Narrow, Associated Absorption Lines in Moderate- and Low-Redshift Quasars, 613, 1, 129. doi:10.1086/422974

Wolfe, A. M., Prochaska, J. X., & Gawiser, E. 2003, ApJ, 593, 215. doi:10.1086/376520

Wu, J., Charlton, J. C., Misawa, T., et al. 2010, ApJ, 722, 997. doi:10.1088/0004-637X/722/2/997

Xu, X., Arav, N., Miller, T., et al. 2020, ApJS, 247, 40. doi:10.3847/1538-4365/ab4bcb

Xu, X., Arav, N., Miller, T., et al. 2019, ApJ, 876, 105. doi:10.3847/1538-4357/ab164e

Xu, X., Arav, N., Miller, T., et al. 2018, ApJ, 858, 39. doi:10.3847/1538-4357/aab7ea